On the role of sphericity of falling rock clusters—insights from experimental and numerical investigations

Ge Gao & M. A. Meguid

Landslides
Journal of the International Consortium on Landslides

ISSN 1612-510X
Volume 15
Number 2

Landslides (2018) 15:219-232
DOI 10.1007/s10346-017-0874-z

Springer

Original Paper

Landslides (2018) 15:219–232
DOI 10.1007/s10346-017-0874-z
Received: 30 November 2016
Accepted: 2 August 2017
Published online: 14 August 2017

Ge Gao · M. A. Meguid

On the role of sphericity of falling rock clusters—insights from experimental and numerical investigations

Abstract In this study, the dynamic behavior of rock clusters falling on rough slopes and impacting a vertical barrier is investigated experimentally and numerically using discrete element analysis. A specially designed laboratory setup that involves a flume of adjustable slope lined with a bumpy surface and equipped with an instrumented wall at the toe is used in the experimental investigation. The velocity profiles and impact forces were measured for three inclination angles using two different rock clusters. Three-dimensional discrete element analysis is then conducted to investigate the mechanical behavior of the rockfall and examine the role of sphericity of the rock cluster on the overall behavior of the system. This was achieved by explicitly simulating the complex shapes of the used rocks and the rough surface of the slope. The material coefficient of friction was measured using heap tests, and the results are compared with those obtained numerically using four different particle sphericities. Conclusions are made regarding the effect of slope inclination angle and the volume of the cluster on the impact forces exerted on rigid barriers. This study suggests that rock sphericity plays important roles on the dynamic behavior of the system and should be taken into consideration in simulating rockfall problems.

Keywords Rockfall · Impact force · Rigid barrier · Rock sphericity · Dynamic behavior · Heap test · Coefficient of restitution · Discrete-element method

Introduction

Rockfall is a common gravity-driven mass movement event in mountainous regions. These events usually involve a sudden movement of either a single rock or a group of rocks that become detached from the rock face and can lead to property damage, personal injury, or even loss of life. Mitigation measures are, therefore, critical at these vulnerable locations and may include the installation of flexible rock fences, catchment ditches, and rigid barriers. Understanding the mechanics of rockfall under various conditions is important to the design of these protection systems. Previous studies (e.g., Basson 2012; Wei et al. 2014) and field observations (e.g., Giani et al. 2004; Alejano et al. 2007; Spadari et al. 2012) show that falling rocks experience different types of motions along its path, including free falling, bouncing, rolling, and sliding. The falling trajectory is controlled mainly by the geometry of the slope, the rock shape, and the energy dissipated at each contact of the rock with the slope. Using small scale experiments, Glover (2015) concluded that rock shape is a key component in determining the dynamics and runout trajectories of rockfall.

A considerable number of studies have been performed over the last few decades to investigate rockfall dynamics or the impact on protection systems and infrastructure using experimental, analytical, and numerical methods (e.g., Ritchie 1963; Erismann 1986; Azzoni et al. 1995; Dorren et al. 2004; Wang and Cavers 2008; Tagliavini et al. 2009; Chen et al. 2013; Lambert et al. 2013; Thoeni et al. 2014; Mateos et al. 2016; Mavrouli et al. 2017).

Discrete element method (DEM) has demonstrated efficiency in replicating rockfall trajectories in addition to modeling crack propagation and breakage of the falling body. McDowell et al. (2011) and Li et al. (2012) used three-dimensional DEM to simulate the movement of gravel material along an inclined chute. Although the analysis provided useful information related to the material behavior, the gravel was modeled using uniform four-ball clumps, which resulted in a simplified shape and particle size distribution. Moreover, the surface of the chute was simply modeled using a rigid wall, leading to inadequate simulation of the frictional-collisional dynamic modes usually observed in experiments. Therefore, there is a need for the development of an improved 3D discrete element analysis of the problem that considers the effect of particle sphericity and angularity and the slope surface roughness such that the response of the system is realistically replicated.

Scope and objectives

This research focuses on investigating the dynamics and impact behavior of falling rock clusters on a rough slope considering the role of rock sphericity and angularity on the movement pattern and the forces exerted on rigid barriers. This is achieved using a combination of laboratory experiments and numerical simulations.

Description of the laboratory experiments and summary of the methodology used to measure impact forces for different slope angles and surface conditions are presented herewith. The test results including the recorded trajectories of the monitored rocks and the impact forces induced by two different rock clusters are summarized. A three-dimensional discrete element model is then developed and used to replicate the conditions of the experiments and the performance of the model is validated by comparing the calculated and measured results. The rough surface is modeled using spherical balls arranged in a hexagonal pattern, and a clump generation procedure is developed to reconstitute three Platonic solids—tetrahedron, hexahedron (cube), and octahedron—which varied in sphericities and angularities to represent the rocks used in experiments. Finally, material calibration is conducted using heap tests to determine the essential numerical parameters needed for the analysis including the friction coefficient that governs the rock movement on the rough slope. The results of the experimental and numerical investigations are then analyzed and conclusions are made regarding the dynamics and impact behavior of the rock clusters.

Experimental program

A series of laboratory experiments was performed to investigate rockfall dynamics and impact characteristics for slope angles of 30°, 45°, and 60°. The test setup (depicted in Fig. 1a) consists of an

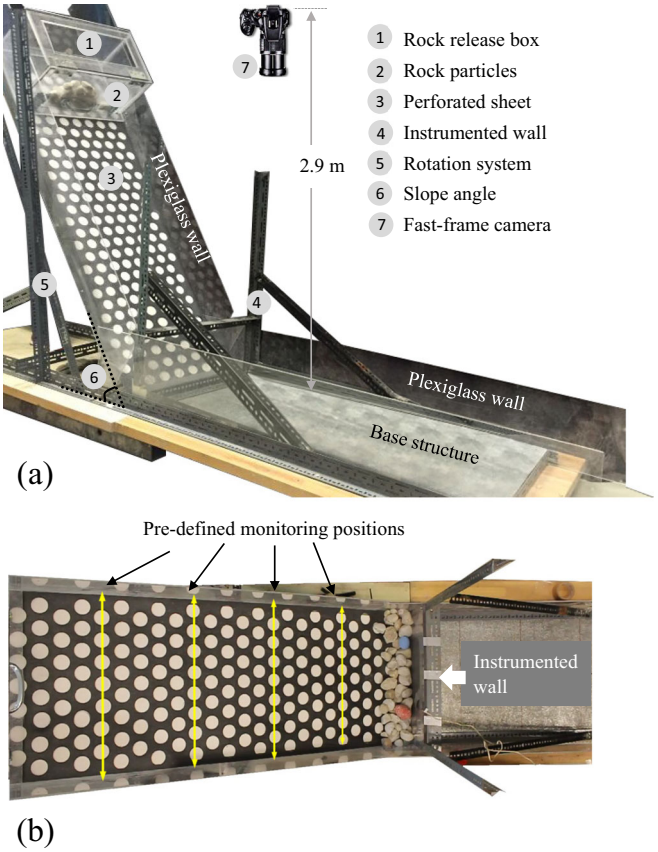

Fig. 1. (a) Experimental setup; (b) Plan view of the slope showing the instrumented wall at the toe

adjustable flume (1.82 m in length, 0.6 m in width and 0.3 m in depth) connected to a horizontal section of equal length with a total width of 0.6 m. The side walls of the flume and the release box located at the top of the slope are made of transparent plexiglass material to allow for the rock movement to be closely monitored using a high-speed camera. Details of the test setup are summarized below.

Perforated sheet

In order to reproduce a realistic slope surface and capture the different modes of rock movement (sliding, falling, rebounding, and rolling), the slope was lined with a specially design rough and bumpy surface. The lining material consists of an ebonite sheet, 1.5 mm in thickness with 5 cm diameter holes arranged in a hexagonal pattern with 8 cm of center spacing (Fig. 1b).

Instrumented wall

A rigid vertical wall made out of plexiglass material fixed into an aluminum frame (0.6 m in width and 0.3 m in height) was fixed at the toe of the slope (Fig. 1b). The wall side facing the slope was instrumented using TactArray pressure sensors (PPS Inc., Los Angeles) with pressure capacity of 345 kPa (50 psi). The sensing pad consists generally of two sets of orthogonal electrode plates separated using a dielectric matrix that acts as a spring allowing for the conformability and stretchability of the pad designs. Each pad contains 256 square-shaped sensing cells arranged in a continuous sheet and controlled using a data acquisition system (Ahmed et al. 2015; Meguid et al. 2017). On the basis of the change of the capacitance between the electrodes, the sensing elements can detect applied loads. In addition to the manufacturer calibration, the sensing pads were also calibrated by placing rock material of known weight (3 kg) and the total weight recorded by the data acquisition system was measured.

Tested material

Previous studies (e.g., Okura et al. 2000; Dussauge et al. 2003; Hantz et al. 2003; Zhang and Yin 2013; Chai et al. 2015) demonstrated that the volume of the falling rock plays an important role in the mechanics of movement and impact on barrier systems. Therefore, two different rock clusters are used in this study as illustrated in Fig. 2. The first cluster (C1) contains 53 particles and measures 0.006 m^3 whereas the second cluster (C2) is almost twice in size with 99 particles and measures 0.01 m^3. In order to ensure consistent particle sizes for both clusters, suitable grain-size distributions are used for both C1 and C2 as shown in Fig. 3. The material consists of pebbles with a maximum diameter of 9.5 cm for C1 and 10.0 cm for C2 with a minimum diameter of 3.0 cm for both clusters. The average particle diameter (d_{50}) is 5.1 and 5.3 cm for C1 and C2, respectively, and the uniformity coefficient (C_u) is 1.52 for both clusters.

Sphericity and angularity

Rock sphericity is known to have a significant effect on the rockfall behavior (Wang and Lee 2010). The sphericity (Eq. 1) is defined by Wadell (1932) as

$$\psi = \frac{\pi^{\frac{1}{3}}(6V_p)^{\frac{2}{3}}}{A_p} \tag{1}$$

where V_p and A_p are the volume and surface area of the particle, respectively. The maximum value obtained using this equation is 1.0 which corresponds to the shape of a sphere. All other shapes have values less than 1.0. In this study, the sphericity was determined using the "intercept method" (Krumbein 1941). For each of the four monitored rock particles, three independent diameters are measured: long, a, intermediate, b, and short, c, as illustrated in Fig. 4a–d. The two ratios (b/a) and (c/b) were calculated to find the sphericity of the particle.

The angularity represents the condition of the particle corners which is considered to be independent of the surface area to volume ratio. The roundness expression (Eq. 2) proposed by Blott and Pye (2008) was utilized in this study.

$$\rho = \frac{N}{\sum\left(\frac{R}{r}\right)} \tag{2}$$

where is r is the radius of curvature of a particle corner, R is the radius of the maximum inscribed circle in the measurement plane, and N is the number of corners in the investigated particle in the same plane.

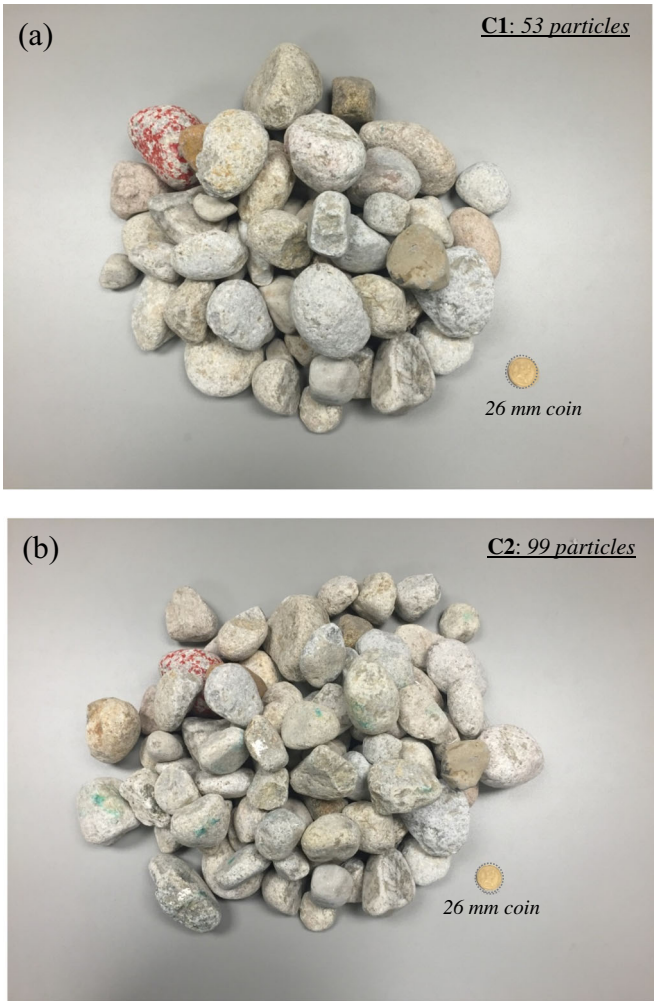

Fig. 2. The tested material: (**a**) cluster C1; (**b**) cluster C2.

The degree of roundness has been used in reference to the smooth curvature of the outline of a plane or a projection area. A plane corner is considered to have reached its maximum degree

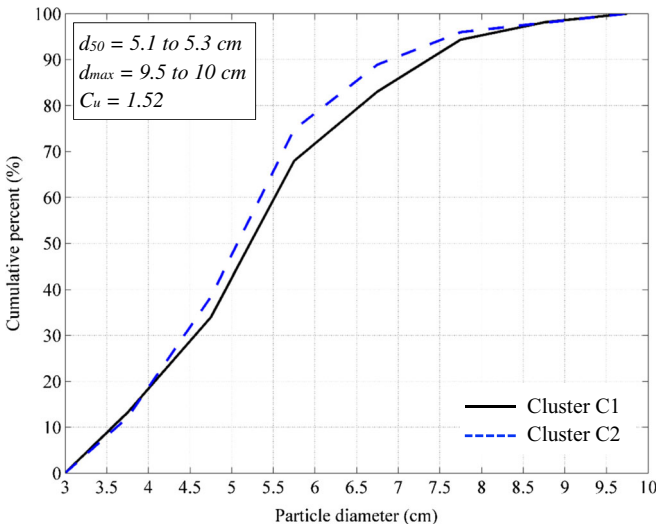

Fig. 3. Particle size distribution of the two rock clusters used in the experiments

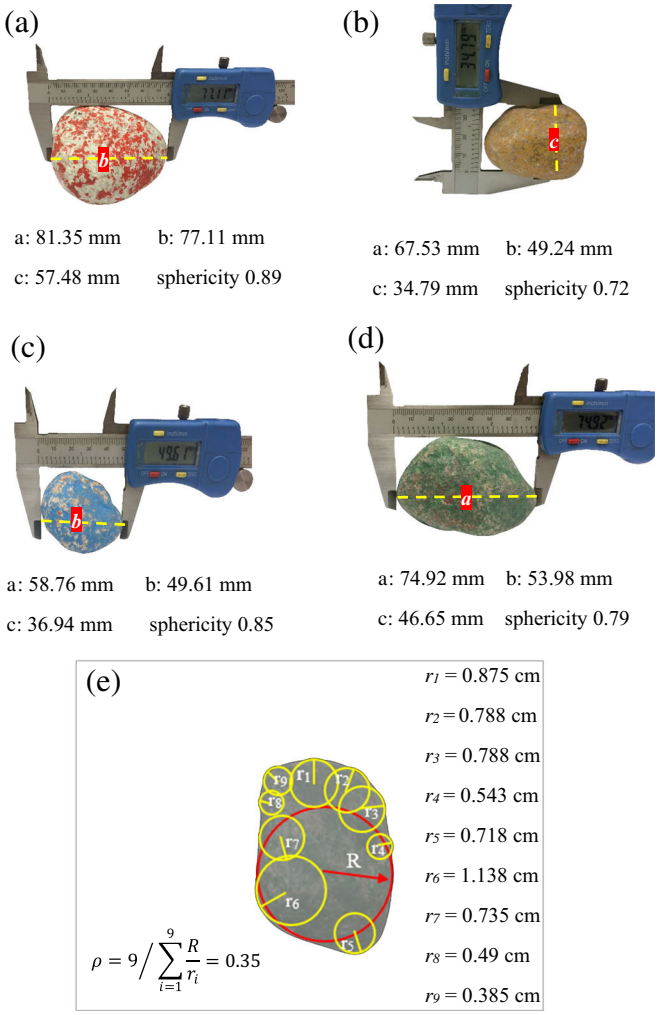

Fig. 4. (**a** through **d**) Measuring the sphericity for the monitored rocks; (**e**) An example illustrating the process used to determine the roundness of one rock.

of roundness when the radius of its smooth curvature equals the radius of the maximum inscribed circle (Wadell 1932). An example illustrating the process used to determine the roundness of one of the monitored particles is presented in Fig. 4e.

The average roundness of the used rock particles was determined using the above procedure and was found to be 0.38 and 0.39 for clusters C1 and C2, with standard deviation of 0.033 and 0.037, respectively. Due to the narrow range of variability in the angularity of the rock material used in this study, more emphasis is placed on the sphericity of the rock cluster.

Test procedure

Prior to each test, the rock particles were held in the transparent release box and allowed to travel down the slope and towards the rigid barrier. For the purpose of capturing the rockfall dynamics, four representative rocks were selected from each cluster and painted in different colors (red, yellow, blue, and green) to facilitate particle tracking during the experiments. The tests were conducted for three different slope inclination angles, namely, 30°, 45°, and 60° for each of the studied rock clusters.

Rock mobility was recorded for each test using high speed video camera (Canon T3i) located at a distance of about 2.9 m above the base of the slope and remotely controlled using a computer unit such that recording is synchronized with the release of the rock cluster. A special software is then used for the digital image analysis after the completion of each experiment. The velocity of the moving rocks is determined by subdividing the recorded videos into still images taken at time intervals of 0.04 s. Similar approach was used by Bozzolo and Lugano (1986), Giani et al. (2004), and Wyllie (2014) for the interpretation of rockfall movement results. The impact forces exerted by the rock on the vertical barrier are measured using the tactile sensing pad placed against the wall and connected to a data acquisition system.

Using digital image processing, the rock velocity is obtained by tracking the position of the rock centroids with respect to a Cartesian coordinate (*X*-*Y*) system for each slope inclination angle. The four marked rocks were monitored using the camera located above the slope as illustrated in Fig. 5a. It should be noted that since the top of the slope is located closer to the camera, the slope width appears larger near the top and decreases gradually with distance from the camera. This geometric distortion has been corrected as shown in Fig. 5b to maintain the same width along the entire slope.

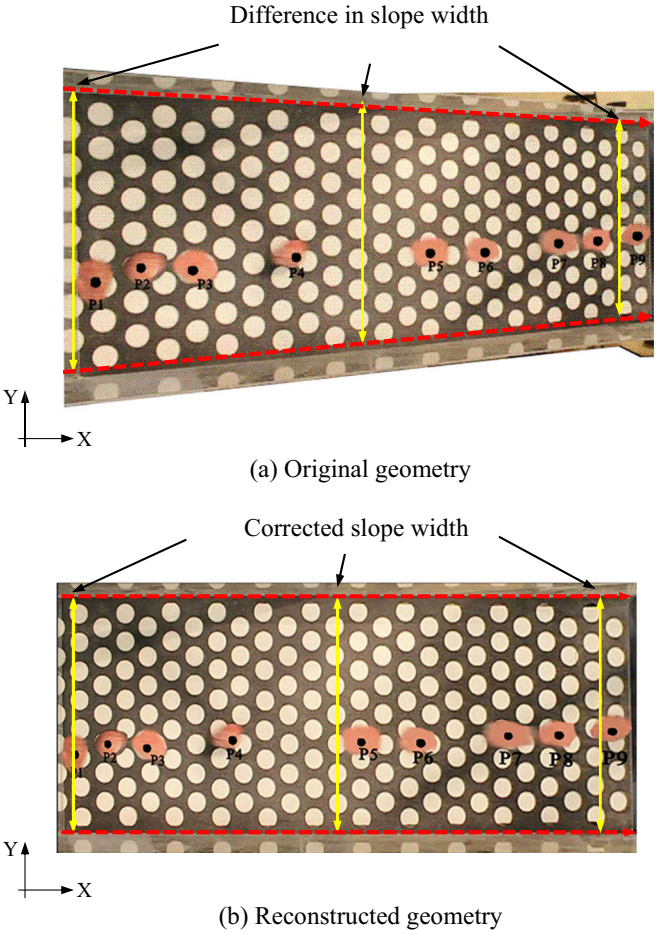

Fig. 5. Top view of the slope **a**) original geometry **b**) reconstructed geometry

Discrete element analysis

Particle flow code (PFC^{3D}) has been used throughout this study to model the three-dimensional behavior of the rock cluster as it moves down the bumpy slope. Translational and rotational motions are determined using Newton's second law and the contact forces caused by the relative movement of particles are updated using force-displacement relationships at each contact point (Potyondy and Cundall 2004). The translational and rotational motions can be generally described using the following equations

$$m_i\left(\frac{d^2x_i}{dt^2}-g_i\right)=\sum_{j=1}^{n_i}\left(F^l_{n,ij}+F^l_{s,ij}+F^d_{n,ij}+F^d_{s,ij}\right) \tag{3}$$

and

$$I_i\frac{d^2\theta_r}{dt^2}=\sum_{j=1}^{n_i}\frac{dH_i}{dt} \tag{4}$$

where m_i, x_i, and I_i are, respectively, the mass, the location, and the moment of inertia of particle *i*. Gravitational and inter-particle forces between particles *i* and *j* in Eq. (3) involve normal and shear components of the elastic forces $F^l_{n,ij}$ and $F^l_{s,ij}$ and similar components of the damping forces $F^d_{n,ij}$ and $F^d_{s,ij}$. In Eq. (4), θ_r represents the relative rolling angles between two contacting particles *i* and *j* and H_i is the angular momentum of the particle.

Clump template and sphericity

Realistic particle shapes play an important role in representing the material behavior using DEM (Taghavi 2011). An individual particle of irregular shape can be simulated in 3D by clumping spheres of different sizes. The resulting clump is a rigid entity with deformable boundary that consists of rigid spherical pebbles overlapping without generating contact forces. Wensrich and Katterfeld (2012) used binary and ternary clumps to simplify particle shape in a repose angle modeling tests. Indraratna et al. (2014) created a subroutine using *MATLAB* to build clump templates based on the radii and coordinates of the spherical balls in a Cartesian system. Albaba et al. (2015) developed a relation between particle microstructure and the loading applied by a granular flow to a rigid wall. Lu and McDowell (2010) used ten-ball tetrahedral clumps with eight asperities to represent the irregular shape of railway ballast in a triaxial test. Cho et al. (2007) used clumped particles to predict the complete nonlinear failure envelope of granite material and synthetic rock. Indraratna et al. (2010) also studied the behavior of railway ballast by projecting images of each stone in two-dimensional space.

In this study, the rocks were modeled using four distinct clump templates of different shapes (10-ball tetrahedral clump, 27-ball cubic clump, 19-ball octahedral clump, and a sphere). The sphericities and angularities were selected to resemble the shapes of the rock used in the experiments, as illustrated in Fig. 6. The sphericities of the Platonic solids (tetrahedron, cube, and octahedron) as well as ideal sphere are determined using Eq. (1) and are presented in Fig. 6a–d, respectively.

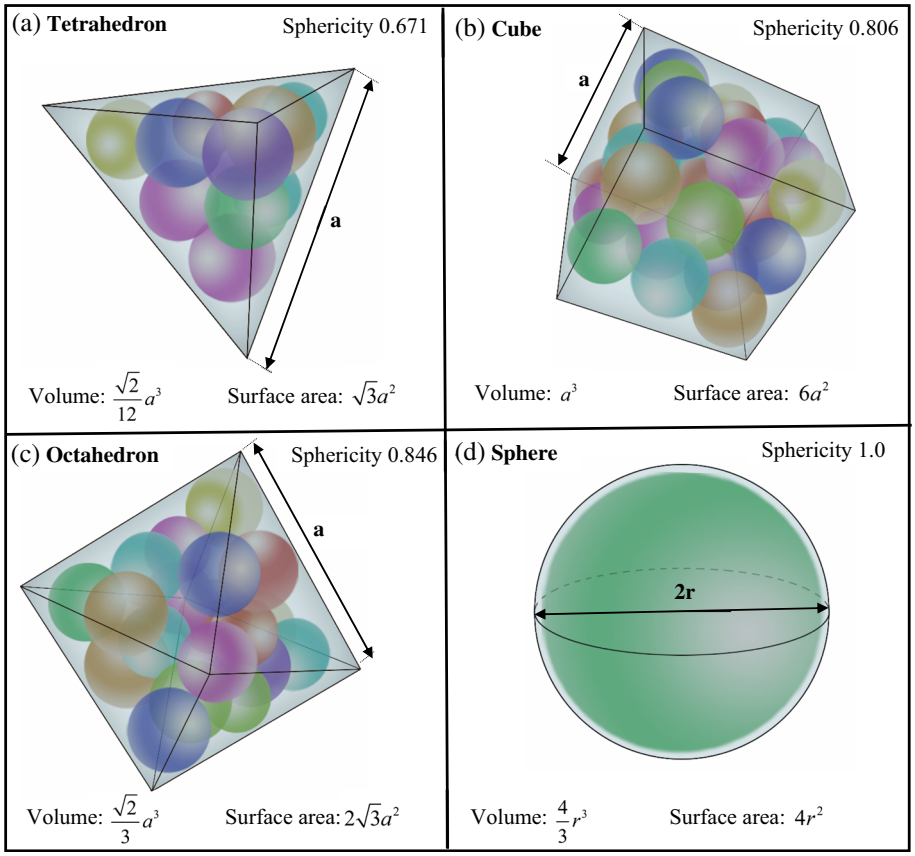

Fig. 6. Platonic-solids used to build clumps of different sphericity for the PFC3D analysis

Angle of repose test

Heap tests have been used by researchers to determine the angle of repose and inter-particle friction coefficient needed for the DEM analysis (e.g., Stahl and Konietzky 2011; Ferellec and McDowell 2010; McDowell et al. 2011). In this study, a total of 35 laboratory heap tests are conducted on the rock material using a glass funnel 17.4 cm in diameter and 40 cm in height placed above a perforated sheet and the average angle of repose of the heap was measured as illustrated in Fig. 7. Experimental results revealed that the material has an average angle of repose of about 25.2°.

A discrete element analysis of the repose angle test was then performed using PFC^{3D} (Itasca Consulting Group 2014) where the funnel was modeled using a cylindrical wall, and the perforated sheet was simulated using solid spheres arranged in a hexagonal pattern. To ensure an optimal spreading of the material, the funnel was lifted using a small velocity of 0.0075 m/s as suggested by Stahl and Konietzky (2011). The effect of sphericity, brought about by the particle shape, on the rolling resistance was examined by performing a series of tests using spherical shaped particles, and the results are compared with those obtained using the created clump templates. Initially, a very small friction coefficient was used to produce a relatively dense state (Itasca Consulting Group 2014) considering linear contact model and effective modulus of 400 MPa such that all possible contact would be rigid. The friction coefficient was incrementally changed to bring the calculated angle of repose close to the average measured value. Figure 8 illustrates the relationship between the calculated particle friction coefficient and angle of repose using the Platonic-solid clumps and spherical particles. Based on the experimental results, the friction coefficients in pebble-pebble contact mode that corresponds to an angle of repose of 25.2° are found to be approximately 0.55, 0.35, and 0.25 for 10-ball tetrahedral, 27-ball cubical, and 19-ball octahedral clumps, respectively. When spherical particles are used to model the heap test, the rolling resistance does not essentially exist and, therefore, the maximum angle of repose is found to be about 21° and the corresponding friction coefficient was about 0.9.

Coefficient of restitution and drop tests

One of the most crucial input parameters controlling rockfall analysis is the coefficient of restitution (Chau et al. 2002; Lo et al. 2010; McDowell et al. 2011). In general, the coefficient of restitution (COR) is defined as the decimal fractional value representing the ratio of velocities before and after an impact of two colliding entities or a body and a rigid surface. The various definitions of the COR including kinematic, kinetic, and energy coefficients are expressed in Eqs. (5)–(7), of which the kinematic coefficient of restitution derived from the lumped-mass (or stereomechanical) impact theory is the most commonly used for rockfall applications (Asteriou et al. 2012).

Kinematic coefficient of restitution

$$\alpha = \sqrt{\frac{H_r}{H_i}} \text{ or } \alpha = \frac{V_r}{V_i} \tag{5}$$

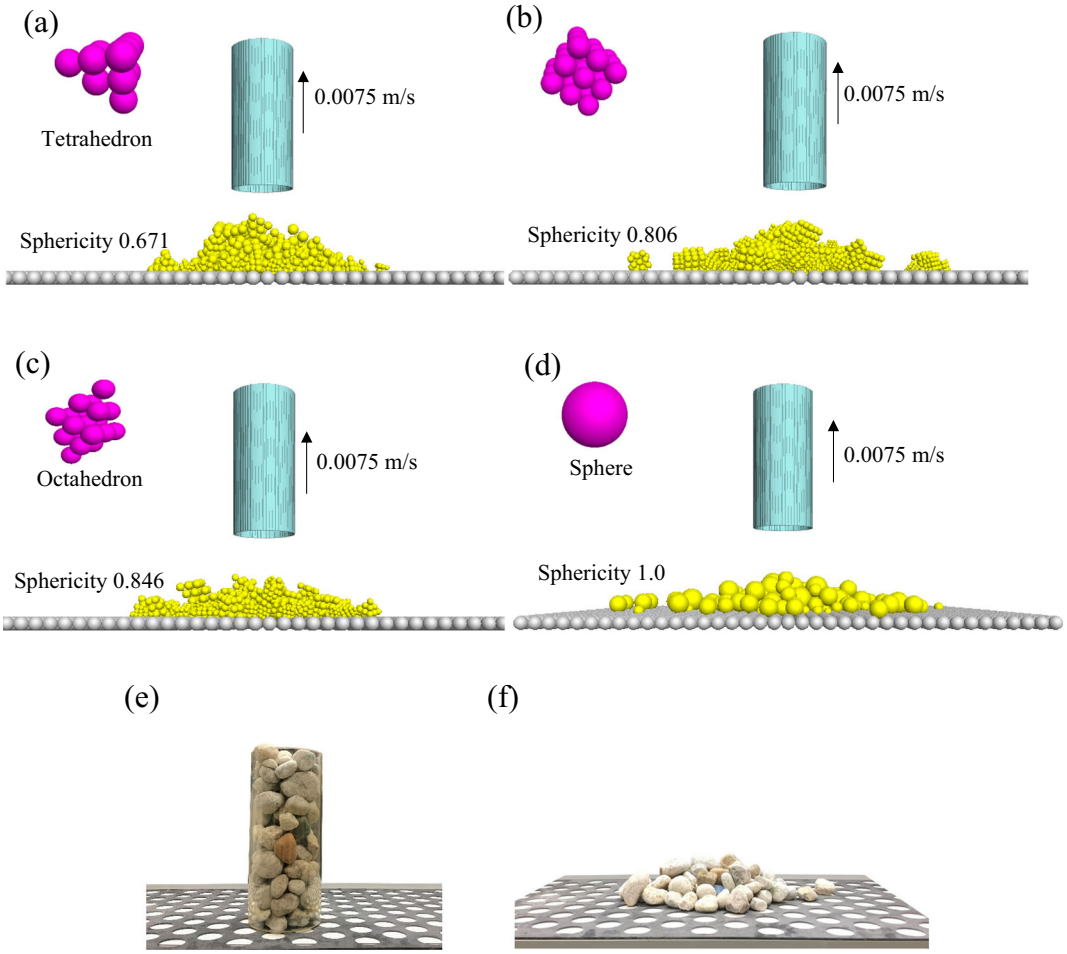

Fig. 7. Experimental and numerical modeling of the repose angle tests: (**a**) 10-ball tetrahedral clumps; (**b**) 27-ball cubic clumps; (**c**) 19-ball octahedral clumps; (**d**) sphere; (**e**) & (**f**) experimental observations

where H_r is the rebound height, and H_i indicates the drop height; V_r and V_i are the magnitudes of the post- and pre-collision velocities, respectively.

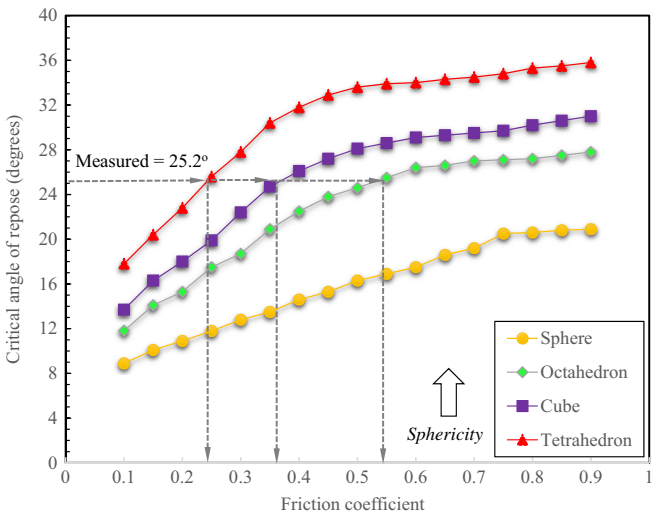

Fig. 8. Relationship between the angle of repose and friction coefficient for different rock shapes

The *kinetic* coefficient of restitution:

$$\alpha = \frac{P_t}{P_n} \tag{6}$$

where P_t and P_n denote the tangential and normal impulses, respectively.

The *energy* coefficient of restitution:

$$\alpha = \frac{E_r}{E_i} = \frac{\frac{1}{2}mV_r{}^2}{\frac{1}{2}mV_i{}^2} = \frac{V_r{}^2}{V_i{}^2} \tag{7}$$

where E_i and E_r are the translational energies before and after impact, and m is the particle mass.

The coefficient of restitution, α, determines the energy loss on collision. In this work, a viscous damping system is used to model the coefficient of restitution by adding normal and shear dashpots at each contact. This damping system is characterized by the critical damping ratio β, given by (Itasca Consulting Group 2014)

$$\beta = \frac{c}{c_c} \tag{8}$$

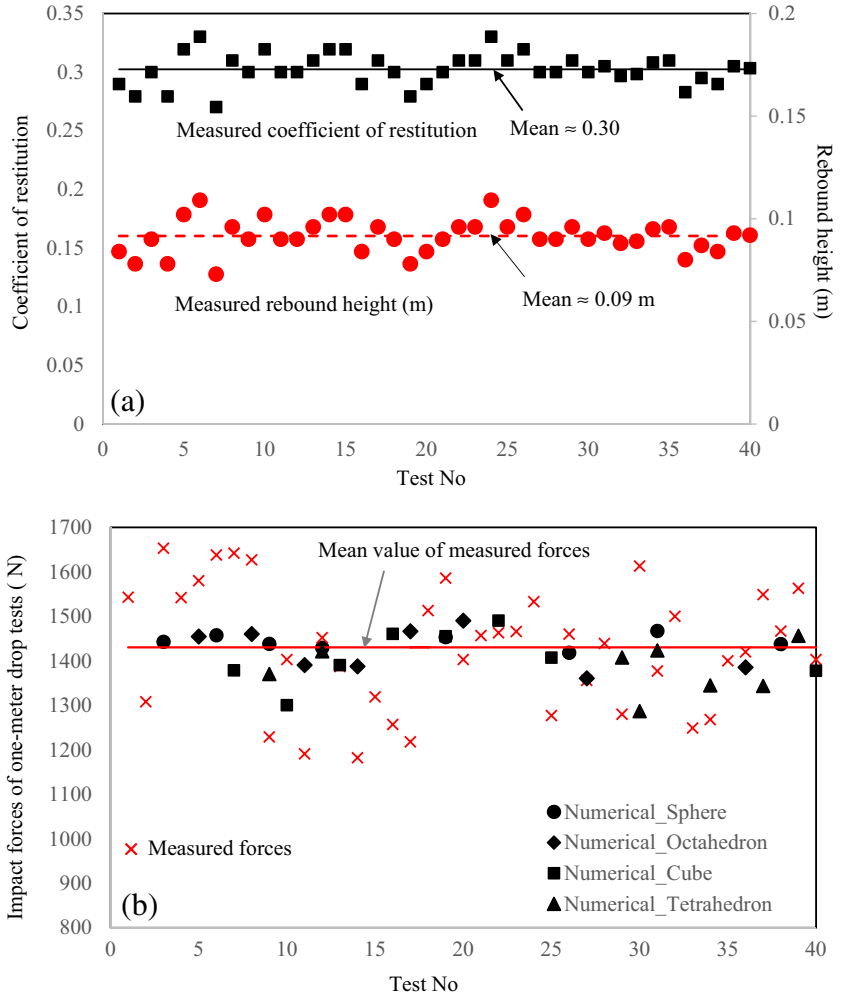

Fig. 9. (**a**) Measured COR using one-meter drop tests; (**b**) Measured vs calculated peak impact forces generated by gravel particles of different sphericities.

where $c = \frac{2\sqrt{mk}\ln(\alpha)}{\sqrt{\ln^2(\alpha)+\pi^2}}$ defined as the damping constant (coefficient of viscous damping), and $c_c = 2m\sqrt{\frac{k}{m}} = 2\sqrt{km} = 2m\omega_n$ defined as the critical damping constant.
where k is the stiffness, and ω_n is the natural frequency of the system.

The coefficient of restitution α is related to the critical damping ratio β such that

$$\alpha = e^{-\frac{\beta\pi}{\sqrt{1-\beta^2}}} \tag{9}$$

Correlation between the kinematic coefficient of restitution, α, and the critical damping ratio, β, was determined in this study using drop tests carried out by allowing rock particles to drop freely at a set distance of 1 m above the surface. An average COR value of 0.30 was obtained based on 40 laboratory tests. The experimental results including the measured rebound heights used to calculate the kinematic COR are shown in Fig. 9a. A summary of all measured and calculated impact forces is presented in Fig. 9b. The observed scatter in the experimental data could be attributed to the random variations in the geometry of individual rock particles (Perera et al. 2016). The mean of the impact forces measured in the laboratory was found to be generally consistent with that calculated using numerical analysis. It is worth noting that the forces calculated for the spherical shaped particles were just around the mean value as compared to those calculated for other shapes (tetrahedrons and cubes) with relatively low sphericities. This can be explained by the approximate geometric representation of these rock particles in the DEM simulation.

To further illustrate the effect of particle shape on the critical damping ratio and the overall response to drop tests, numerical simulations were performed using Platonic-shaped clumps of different sphericities as illustrated in Fig. 10. The critical damping ratio was found to vary from 0.0 to 1.0 as x increases. The maximum rebound height was calculated for particles close to x = 0.0 where no energy dissipation exists during impact. A summary of the micromechanical parameters needed for the DEM simulation is given in Table 1. It is noted that the effective contact modulus E_c used in this study is based on that reported by Stahl and Konietzky (2011).

The relationship between the kinematic restitution coefficients and damping ratios using both spheres and irregular shaped clumps is presented in Fig. 11. The measured kinematic COR value is used to determine the corresponding damping ratio for each shape. The critical damping ratio was found to be approximately

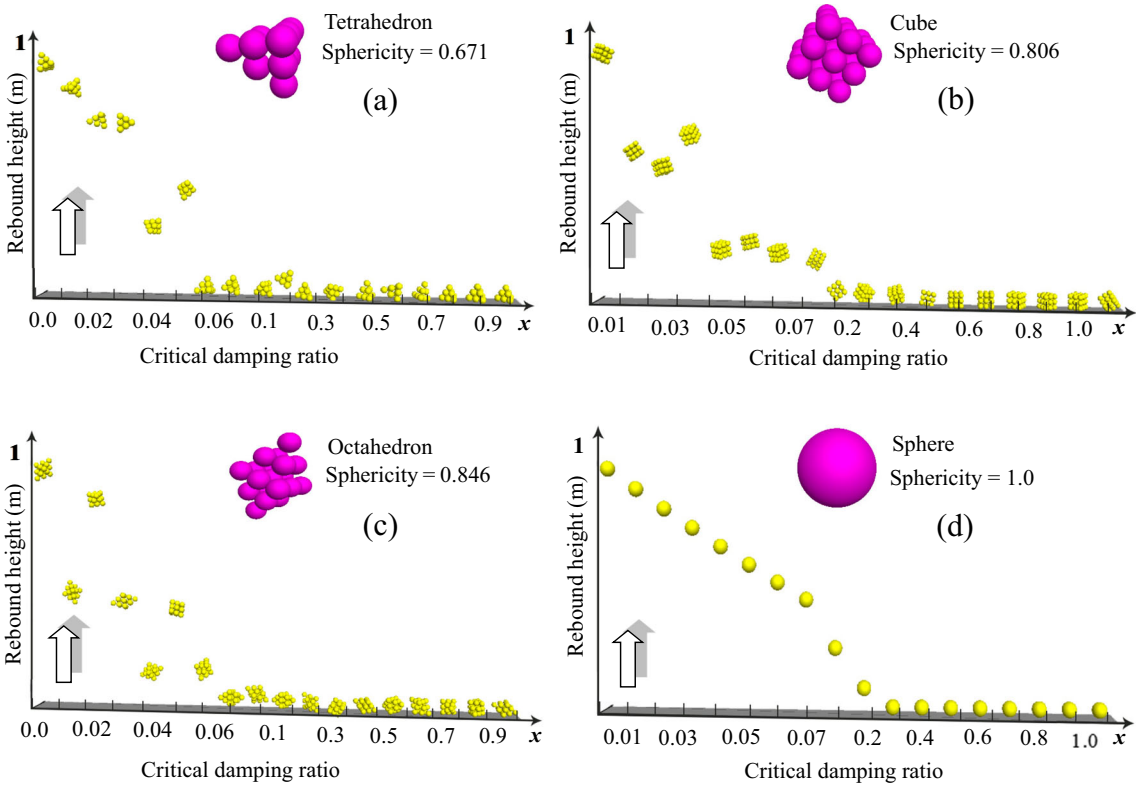

Fig. 10. DEM simulation of the drop tests using: (**a**) 10-ball tetrahedral clump; (**b**) 27-ball cubical clump; (**c**) 19-ball octahedral clump and (**d**) sphere.

0.19, 0.23, 0.27, and 0.35 for the 10-ball tetrahedral, 27-ball cubical, 19-ball octahedral, and spherical shaped particles, respectively.

Rockfall dynamics

Discrete element simulations of the experiments are performed to understand the role of various parameters on the mobility of the moving particles. It is worth noting that all the microparameters are adopted from Table 1. To simulate the presence of perforated sheet along the slope, a fixed hexagonal closed grain layer made out of 4880 spherical particles was created so that the movement of the rock cluster down the slope is properly simulated. This is particularly true for the rolling behavior that is achieved through successive particle collisions with the grain layer generated along the slope (Lo et al. 2010). To investigate the importance of sphericity in rockfall dynamics, the diameters of the spheres within the clump and the spherical shaped rock were determined by equating their volume with that of the rocks used in the experiments (McDowell et al. 2011). The simulations were performed using two different clusters (C1 and C2) initially contained within four rigid walls representing the release box located at the top of the slope. The numerical procedure used to simulate the experiment is illustrated in Fig. 12 for the three investigated slope angles. The rock cluster was released by deleting the front face of the wall and turning on gravity for all particles. The marked rocks were generated in various simulations using the clump templates and placed such that the initial locations match that of the experiments.

Effect of sphericity

The behavior of a single rock moving on 30° slope is first investigated using spherical as well as Platonic-shaped particles. Figure 13 depicts the calculated particle trajectories using the developed discrete element model for different particle shapes. The trajectory resulting from the movement of a rock particle modeled using 10-ball tetrahedral clump with a relatively low sphericity (0.671) is found to be predominantly governed by sliding. On the other hand, the 27-ball cubical clump (sphericity = 0.806) and 19-ball octahedral clump (sphericity = 0.846) exhibited movement patterns that are dominated by rolling and bouncing (see in Fig. 13b, c). The results also showed that the trajectory resulting from the 19-ball octahedral clump (sphericity = 0.846) showed a pronounced combination of sliding, rolling, and bouncing as compared to the trajectory of the 27-ball cubic clump (sphericity = 0.806).

Using a simplified spherical particle (sphericity = 1.0) to represent the rock resulted in a movement pattern that is characterized

Table 1 Parameters used in the discrete element analysis

Input parameters for DEM simulation				
Density (kg/m^3)	Contact (MPa)	Stiffness ratio (k_n/k_s)	Friction coefficient	Angle of repose (°)
2620	400	1.5	0.4	28

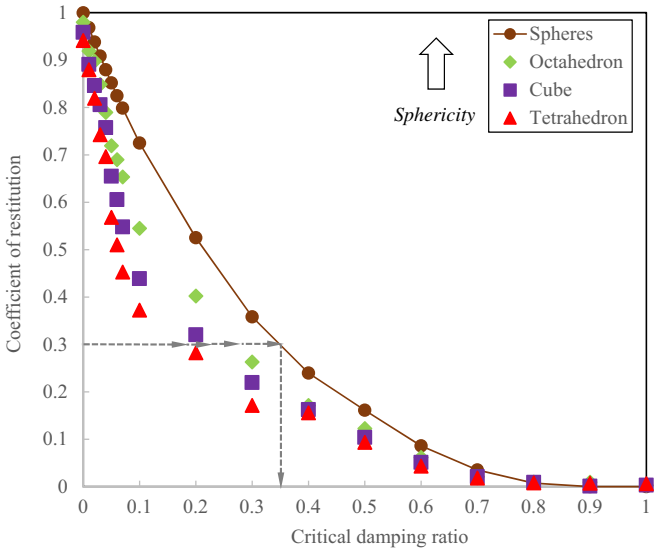

Fig. 11. Relationship between the coefficient of restitution and critical damping ratio for different rock shapes

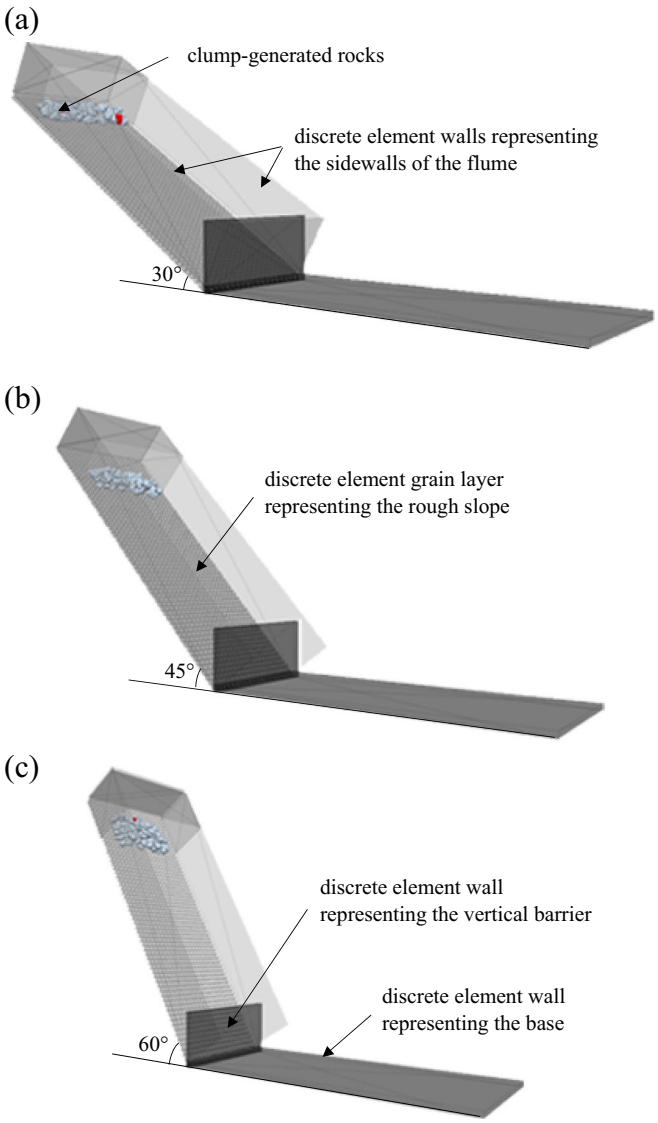

Fig. 12. The numerically generated model for slope angles of: (**a**) 30°; (**b**) 45° and (**c**) 60°.

by sliding and repeated bouncing after touching the slope with tendency of easily detaching from the slope (Fig. 13d). This is attributed to the fact that less energy is lost in this case due to the absence of rolling resistance.

To further illustrate how sphericity affects the dynamics of the rock cluster, the discrete element results obtained from the analysis of cluster C2 is shown in Fig. 14 for inclination angle of 60°. For 10-ball tetrahedral clumps (that represents the lowest sphericity), the marked rock was found to be located at a horizontal distance of 0.38 m away from the toe of the slope at elapsed time of 0.40 s as shown in Fig. 14a. The location of the tracked particle in the cluster at the same elapsed time was found to be 0.29 and 0.23 m from the toe for the 27-ball cubic and the 10-ball octahedral clumps, respectively (Fig. 14b, c). For spherical particles (Fig. 14d), at the same time stamp, the entire rock cluster had already traveled to the toe of the slope.

Effect of cluster size

Figure 15 compares the measured and calculated velocity profiles for the two investigated clusters (C1 and C2). As the slope angle increases, the difference between the velocity calculated using Platonic-shaped clumps and spherical particles gradually diminishes particularly near their maximum values at a distance of about 1.4 m from the release box. For high inclination angles, the dynamics of the rockfall was found to be predominantly governed more by falling motion than rolling and sliding.

By inspecting Fig. 15a, b, it can be seen that for slope angle of 30°, the measured and calculated velocity profiles are influenced by the cluster size, whereas for inclination angles of 45° and 60° (Fig. 15c, d, e, f), the difference in velocities for the two used clusters became insignificant. The average calculated velocity for the monitored (red) rock in C2 with the highest sphericity (0.89) in the cluster is found to be about 6% larger than that observed for the same rock in C1 for 30° inclination angle. Similarly, the velocity measured for the monitored (yellow) rock with the lowest sphericity (0.72) in cluster C2 is found to be about 8% higher compared to that observed in cluster C1. As the slope angle increased to 45° and 60°, the average velocity of the monitored (red) rock with sphericity of 0.89 is 4.5 and 1.3% higher for C2 compared to C1, respectively. Similar trend was found for the monitored (yellow) rock with sphericity of 0.72.

The numerical results also revealed that when the sphericity is relatively low, the effect of the volume of the rock cluster is more pronounced. For, instance, for slope angle of 30°, the velocities of the four marked rocks: red (0.89), blue (0.85), green (0.8) and yellow (0.72) in cluster C2 are higher by 5.9, 6.7, 7.4, and 8.1%, respectively, as compared to C1. This is attributed to the fact that low sphericity rocks have relatively more chances to dissipate kinetic energy as a result of the higher rolling friction caused by its shape compared to spherical shaped rocks.

Effect of slope inclination angle

By examining the measured velocity profiles for clusters C1 (Fig. 15a, c, e) and C2 (Fig. 15b, d, f), it can be seen that as the slope angle increased, the velocity of all monitored particles increased. When the

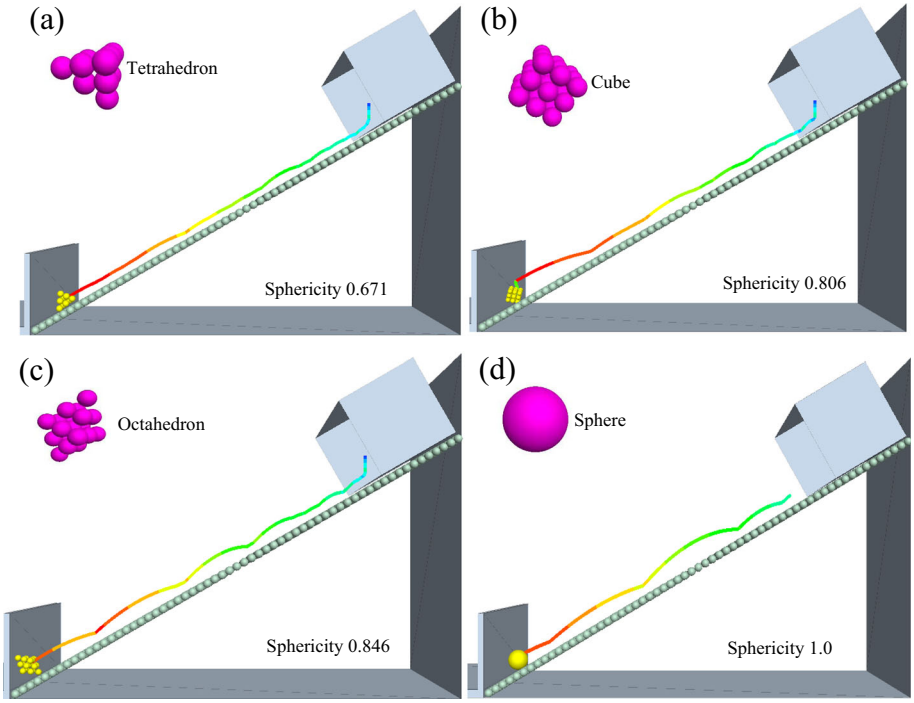

Fig. 13. Rockfall trajectories resulting from the release of different shaped-particles on a rough surface for: (**a**) 10-ball tetrahedral clump; (**b**) 27-ball cubic clump; (**c**) 19-ball octahedral clump and (**d**) sphere.

traveled distance reached about 1.1 m, the calculated velocities of the red rock (sphericity = 0.89) in cluster C1 reached 3.1, 4.0, and 5.1 m/s for slope angles 30°, 45°, and 60°, respectively. The velocities of the same rock in cluster C2 at the same location are found to be slightly higher (3.5, 4.3, and 5.2 m/s) for the three slope angles.

As the rock sphericity increased, the velocity of the four monitored rocks: red (0.89), blue (0.85), green (0.8), and yellow (0.72) increased for both clusters. For 30° slope, when the traveled distance reached 1.4 m, the velocities of the red, blue, green, and yellow rocks reached 3.9, 3.5, 3.2, and 2.6 m/s,

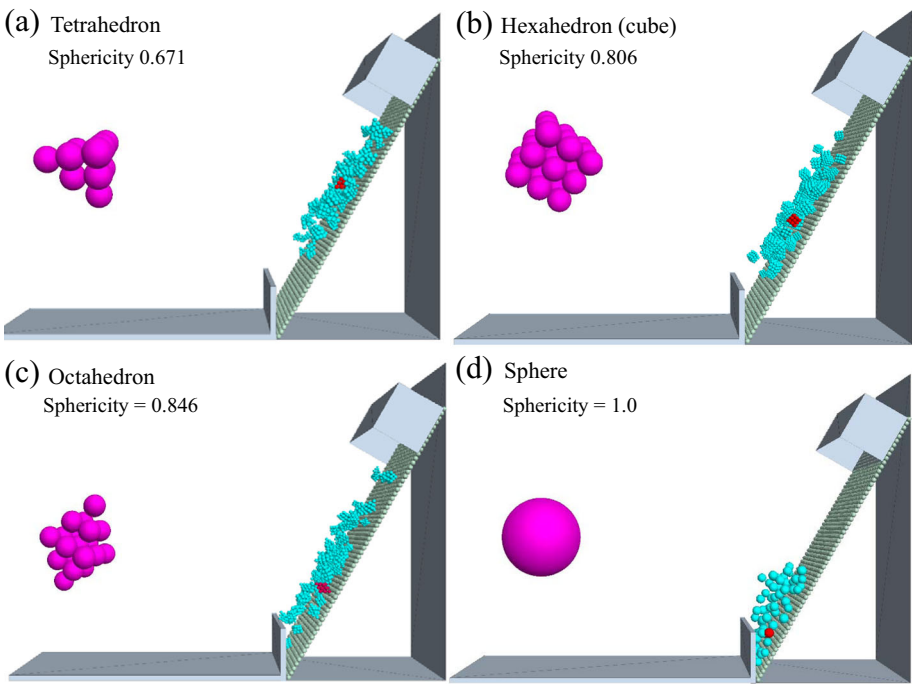

Fig. 14. A snapshot showing the movement of cluster C2 and the calculated locations of the marked particles for slope inclination angle of 60°

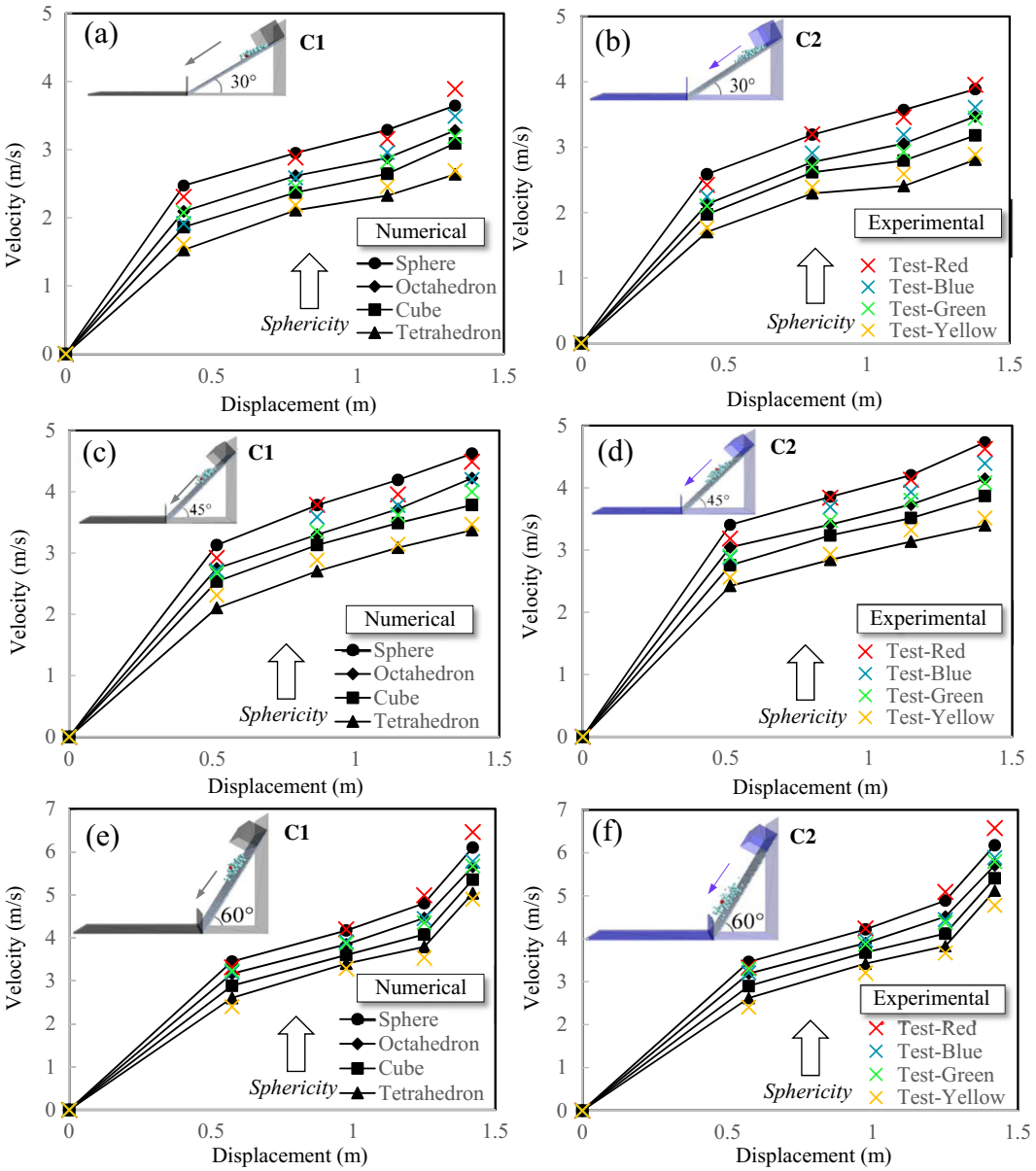

Fig. 15. Measured and calculated velocity profiles using spherical and clump particles for different clusters and inclination angles.

respectively, for C1 and 4.0, 3.7, 3.4, and 2.8 m/s, respectively, for C2. Increasing the slope angle to 45° resulted in an increase in the rock velocities reaching 4.5, 4.2, 4.0, and 3.5 m/s for C1 and 4.7, 4.5, 4.1, and 3.5 m/s for C2. With further increase in slope angle to 60°, the measured velocities were found to be 6.4, 5.8, 5.6, and 4.9 m/s, respectively, for C1 and 6.6, 5.9, 5.7, and 5.0 m/s for C2.

Comparing the experimental results for the monitored rock particles (that have different sphericities) with the numerical simulations based on the examined shapes (tetrahedral, cubic, octahedral, and sphere), the velocities of the particles were found to be overall consistent. For example, when considering the effect of cluster size and slope inclination angle, the velocity profile of the monitored yellow particle with the lowest sphericity (0.72) was found to be consistent with the velocity profile of the tetrahedral clumps, which also has the lowest sphericity (0.671) among the examined Platonic-solid clumps as shown in Fig. 15.

To illustrate the role of the slope angle on the dynamics of the investigated rockfall problem, the location of the rocks in cluster C2 is examined for different inclination angles that are depicted in Fig. 16. For inclination angle of 30° (Fig. 16a), the position of the marked rock at elapsed time of 0.40 s was found to be mainly in the upper half of the slope. The location of the rock changed at the same elapsed time when the slope angle increased to 45° (Fig. 16b). For 60° angle, the entire volume had already traveled to the end of the slope at the same time stamp. In all investigated cases, the velocity of the moving rocks was found to reach its maximum value at about half way through the slope.

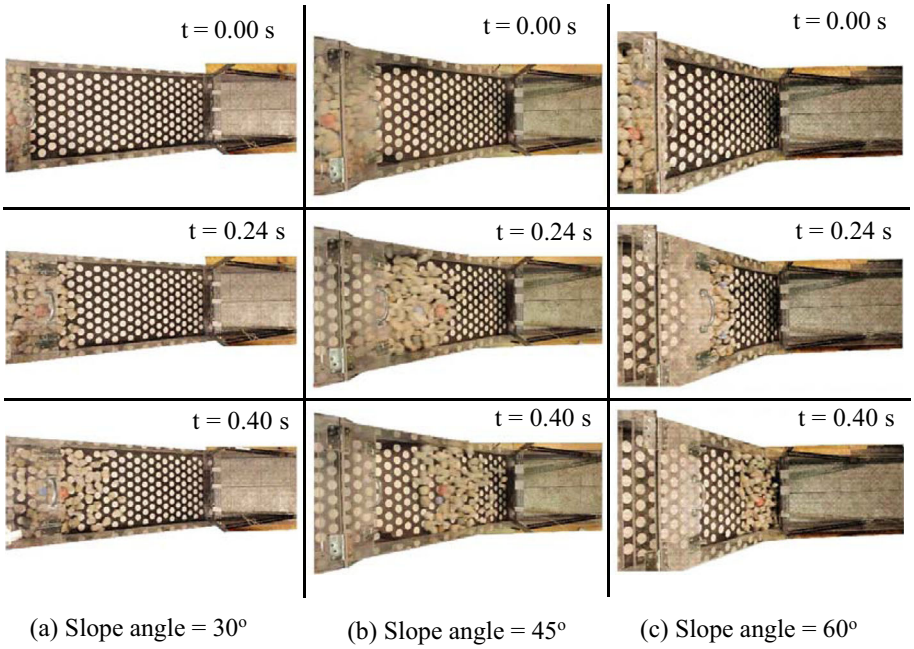

Fig. 16. Sequences of rockfall for different slope angles (cluster C2)

Impact forces on the rigid barrier

Following the model validation, subroutines were developed in PFC^{3D} using the FISH Language such that the impact information of the two investigated rock clusters is fully recorded (e.g., particle IDs, impact time, impact forces in different directions). To evaluate the effect of rock sphericity on the forces exerted on the barrier, the monitored rocks of different sphericities were used to in the analysis in conjunction with the experimental data obtained using the TactArray sensing pads. The impact locations of each of the rocks on the sensors was determined and the magnitudes of the impact forces are then obtained for both clusters. A summary of the changes in impact forces for different slope inclination angles is given in Fig. 17a, b for clusters C1 and C2, respectively. The impact forces generally increased as the slope angle increased. For α = 30°, the impact force of the (red) rock with the highest sphericity (0.89) in the first C1 was found to be about 200 N and further increased to 405 and 821 N when the slope angle reached 45° and 60°, respectively. Similarly, the impact forces of the same rock in cluster C2 are found to be 220, 426, and 838 N for slope angles of 30°, 45°, and 60°, respectively.

The effect of rock sphericity is examined by comparing the impact forces exerted by four different rock models (tetrahedral, cubic, octahedral, and sphere) with increasing sphericity from 0.67, 0.80, and 0.85 to 1.0 as summarized in Table 2. It is worth noting that the computed impact forces using the four different rock shapes are in agreement with the measured results for the monitored rock particles. For instance, for cluster size C2, the impact forces induced by the cubical (sphericity = 0.8) and octahedral (sphericity = 0.85) shaped rocks are found to be 341 and 381 N, respectively, for inclination angle of 45° which are consistent with the measured values for the green and blue rocks (335 and 374 N), which have sphericities of 0.80 and 0.85, respectively. It is also observed that for both clusters, impact forces increased with the increase in particle sphericity. For example, for slope angle of 30°, the impact forces increased by about 43% for the tetrahedral clump, about 58% for the cubical clump, and about 68% for the octahedral clump as compared to the spherical shaped rock. For slope inclination angles of 45°, the increase in the impact forces for the three clump types were found to be 12, 22, and 34%, respectively. These results suggest that, for the investigated rock clusters, the effect of particle sphericity on the impact force decreases as the slope angle increases. For slope angles of 45° or less, both combinations of rolling and bouncing modes govern the cluster movements leading to more pronounced effect of rock shape on the impact forces.

Limitations

It is well known that falling rocks can range from small cobbles to large boulders of several cubic meters in size traveling at speeds of tens of meters per second (Guzzetti et al. 2002). In addition, the geometrical and mechanical characteristics of the slope surface can vary dramatically in different areas (Agliardi and Crosta 2003). The experimental work presented in this study is conceptual in nature and represents an ideal condition that involves small rock particles moving on a uniformly rough slope with only limited number of particles tracked during the experiments. For the sake of simplicity, only four particles were considered for monitoring during the experiments assuming that they represent the movement of the cluster. This was justified by the fact that the river pebbles used in this study were obtained from a single source with similar material and geometric characteristics.

Simplifications were also made in the numerical analysis by using four simple rock shapes to model the rock cluster. It has been reported (Glover 2015) that using Platonic-solid-shaped clumps and spheres may generate different characteristic runout dynamics since the simplified rock shapes may have uniform sphericities and angularities.

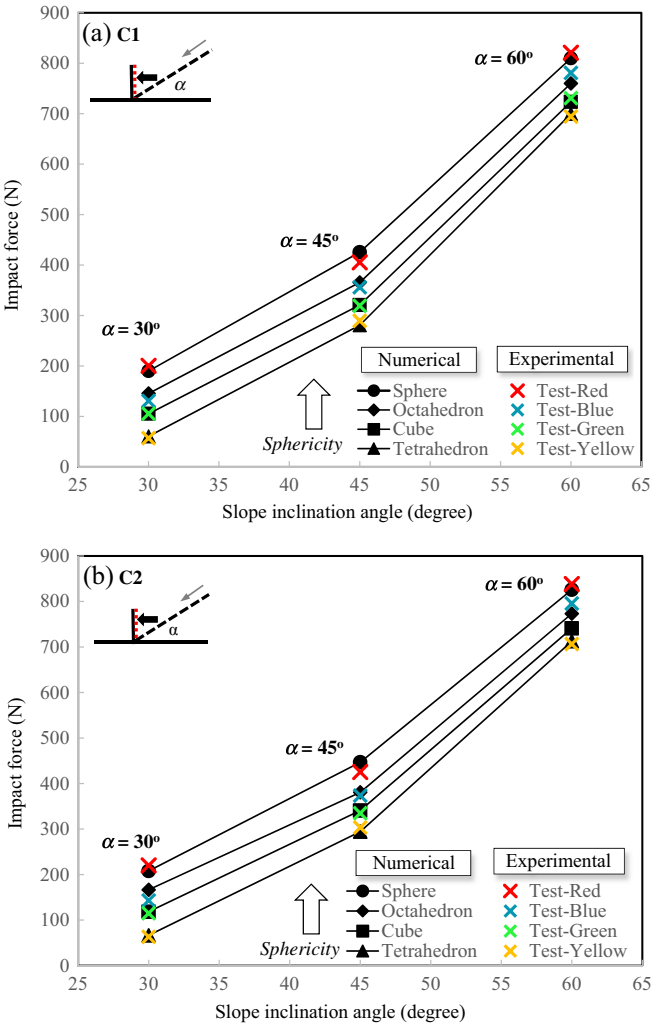

Fig. 17. Calculated and measured impact forces on the barrier at inclination angles of 30°, 45°, and 60° for: (**a**) cluster C1 and (**b**) cluster C2.

Finally, despite the fact that the impact forces exerted by real rockfall events can reach tens of thousands of kilonewton (Pichler et al. 2005), the results in this study are considered to be a step forward towards understanding the role of rock shapes on the impact forces induced by falling rock clusters on nearby structures.

Summary and conclusions

In this study, an experimental investigation was performed to understand the mobility of rockfall on a rough surface for three different slope inclination angles. A series of three-dimensional numerical simulation was conducted using the distinct element code PFC^{3D}. Three Platonic-solid-shaped clumps were used to investigate the effect of sphericity on the dynamic behavior of the falling rock clusters as well as the impact on a rigid barrier wall. The friction coefficient of the rock used in the experiments was determined using heap tests. The calibration involved measuring the repose angle of the rock cluster and establishing a relationship between the angle of repose and the inter-particle friction coefficient. Both clumps and spherical particles were used in the discrete element analysis to fully understand the importance of particle sphericity on the response. The velocity and trajectories of selected rocks were recorded to understand the effect of rock sphericity on the mobility of the clusters. In addition, the impact pressures exerted by the falling rocks on an instrumented wall were examined.

General agreement was found between the recorded and calculated results for the two rock clusters used in this study.

For gentle slopes with inclination angle of 30°, rolling and sliding are found to be the prevalent mechanisms of motion. The increase in slope angle from 30° to 45° and then to 60° resulted in significant changes in the dominant mechanism of movement. When the rock cluster travels over a steep slope, free fall-like and rapid sliding behaviors were consistently observed. It should be pointed out that the difference brought about by the sphericity was not apparent for steep inclination angles. This can be explained by the absence of particle rolling mechanism which is highly affected by both the particle shape and surface roughness.

The effect of rock sphericity on the impact forces was also investigated for two different rock clusters and for the range of slope inclination angles used in this study. The results indicated that for gentle slopes, the higher the sphericity of the falling rock cluster, the less the interaction (and energy loss) among individual particles leading to larger impact forces on the rigid barrier.

Finally, the developed numerical model showed that modeling the particle shapes and the surface roughness of the slope are important to capture the behavior of the falling rock cluster. This modeling approach may be suitable to analyze similar rockfall problems.

Table 2 Effect of particle sphericity on impact forces

Test Type	Rock color	Sphericity	Cluster C1 (0.006 m^3) 30°	45°	60°	Cluster C2 (0.01 m^3) 30°	45°	60°
Physical	Yellow	0.72	60.9	281.6	704.3	63.3	303.4	706.5
	Green	0.80	101.5	315.6	730.8	114.9	334.9	744.9
	Blue	0.85	135.8	356.2	781.5	143.0	373.7	795.6
	Red	0.89	200.3	405.4	821.9	220.2	425.3	838.3
Numerical	Tetrahedral	0.67	60.4	280.3	698.7	66.5	294.3	712.8
	Cubical	0.80	105.2	319.8	723.3	118.4	340.8	741.0
	Octahedral	0.85	145.4	365.7	759.2	166.6	380.7	773.2
	Spherical	1.0	189.9	425.8	808.9	207.9	446.8	825.7

Acknowledgements

This research is supported by the Natural Sciences and Engineering Research Council of Canada (NSERC) under Grant Number 311971-06.

References

Agliardi F, Crosta GB (2003) High resolution three-dimensional numerical modelling of rockfalls. Int J Rock Mech Min Sci 40:455–471

Ahmed MR, Tran VDH, Meguid MA (2015) On the role of geogrid reinforcement in reducing earth pressure on buried pipes: experimental and numerical investigations. Soils Found 55(3):588–599

Albaba A, Lambert S, Nicot F, Chareyre B (2015) Relation between microstructure and loading applied by a granular flow to a rigid wall using DEM modeling. Granul Matter 17:603

Alejano L, Pons B, Bastante F, Alonso E, Stockhausen H (2007) Slope geometry design as a means for controlling rockfalls in quarries. Int J Rock Mech Min Sci 44:903–921

Asteriou P, Saroglou H, Tsiambaos G (2012) Geotechnical and kinematic parameters affecting the coefficients of restitution for rock fall analysis. Int J Roc Mech Min Sci 54:103–113

Azzoni A, Barbera GL, Zaninetti A (1995) Analysis and prediction of rockfalls using a mathematical model. Int J Rock Mech Min Sci 32:709–724

Basson FRP (2012) Rigid body dynamics for rock fall trajectory simulation. American Rock Mechanics Association 12–267

Blott SJ, Pye K (2008) Particle shape: a review and new methods of characterization and classification. Sedimentology 55(1):31–63

Bozzolo D, Lugano PR (1986) Simulation of rock falls down a valley side. Acta Mech 63(1–4):113–130

Chai B, Tang Z, Zhang A, Du J, Su H, Yi H (2015) An uncertainty method for probabilistic analysis of buildings impacted by rockfall in a limestone quarry in Fengshan, Southwestern China. Rock Mech Rock Eng 48:1981–1996

Chau KT, Wong RHC, Wu JJ (2002) Coefficient of restitution and rotational motions of rockfall impacts. Int J Rock Mech Min Sci 39:69–77

Chen G, Zheng L, Zhang Y (2013) Numerical simulation in rockfall analysis: a close comparison of 2-D and 3-D DDA. Rock Mech Rock Eng 46(3):527–541

Cho N, Martin CD, Sego DC (2007) A clumped particle model for rock. Int J Rock Mech Min Sci 44:997–1010

Dorren LKA, Maier B, Putters US, Seijmonsbergen AC (2004) Combining field and modelling techniques to assess rockfall dynamics on a protection forest hillslope in the European Alps. Geomorphology 57:151–167

Dussauge C, Grasso JR, Helmstetter A (2003) Statistical analysis of rockfall volume distribution: implications for rockfall dynamics. J Geophys Res Solid Earth 108:ETG2.1–ETG2.11

Erismann TH (1986) Flowing, rolling, bouncing, sliding, synopsis of basic mechanisms. Acta Mech 64:101–110

Ferellec JF, McDowell G (2010) A method to model realistic particle shape and inertia in DEM. Granul Matter 12:459–467

Giani GP, Migliazza M, Segalini A (2004) Experimental and theoretical studies to improve rock fall analysis and protection work design. Rock Mech Rock Eng 37(5):369–389

Glover J (2015) Rock-shape and its role in rockfall dynamics. PhD thesis. Durham University, Old Elvet, Durham

Guzzetti F, Crosta G, Detti R, Agliardi F (2002) STONE: a computer program for the three-dimensional simulation of rock-falls. Comput Geosci 28(9):1081–1095

Hantz D, Vengeon JM, Dussauge-Peisser C (2003) An historical, geomechanical and probabilistic approach to rock-fall hazard assessment. Nat Hazards Earth Syst Sci 3(6):693–701

Indraratna B, Thakur PK, Vinod JS (2010) Experimental and numerical study of railway ballast behavior under cyclic loading. Int J Geomech 10(4):136–144

Indraratna B, Ngo NT, Rujikiatkamjorn C, Vinod J (2014) Behavior of fresh and fouled railway ballast subjected to direct shear testing: discrete element simulation. Int J Geomech 14(1):34–44

Itasca Consulting Group. (2014). Particle flow code in three dimensions (PFC^{3D}). Minneapolis

Krumbein W (1941) Measurement and geological significance of shape and roundness of sedimentary particles. J Sediment Petrol 11:64–72

Lambert S, Bourrier F, Toe D (2013) Improving three-dimensional rockfall trajectory simulation codes for assessing the efficiency of protective embankments. Int J Min Sci Rock Mech 60:26–36

Li H, McDowell GR, Lowndes IS (2012) A laboratory investigation and discrete element modeling of rock flow in a chute. Powder Technol 229:199–205

Lo CY, Bolton MD, Cheng YP (2010) Velocity fields of granular flows down a rough incline: a DEM investigation. Granul Matter 12:477–482

Lu M, McDowell GR (2010) Discrete element modelling of railway ballast under monotonic and cyclic triaxial loading. Géotechnique 60(6):459–467

Mateos RM, García-Moreno I, Reichenbach P, Herrera G, Sarro R, Rius J, Aguiló R, Fiorucci F (2016) Calibration 30 and validation of rockfall modeling at regional scale: application along a roadway in Mallorca (Spain) and organization of its management. Landslides 13:751–763

Mavrouli O, Giannopoulos PG, Carbonell JM, Syrmakezis C (2017) Damage analysis of masonry structures subjected to rockfalls. Landslides 14(3):891–904

McDowell G, Li H, Lowndes I (2011) The importance of particle shape in discrete element modelling particle flow in a chute. Geotechnique Lett 1(3):59–64

Meguid MA, Hussein MG, Ahmed MR, Omeman Z, Whalen J (2017) Investigation of soil-geosynthetic-structure interaction associated with induced trench installation. Geotext Geomembr. doi:10.1016/j.geotexmem.2017.04.004

Okura Y, Kitahara H, Sammori T, Kawanami A (2000) The effects of rockfall volume on runout distance. Eng Geol 58(2):109–124

Perera S, Lam N, Pathirana M, Zhang L, Ruan D, Gad E (2016) Deterministic solutions for contact force generated by impact of windborne debris. Int J Impact Eng 91:126–141

Pichler P, Hellmich C, Mang H (2005) Impact of rocks onto gravel: design and evaluation of experiments. J Impact Eng 31:559–557

Potyondy DO, Cundall PA (2004) A bonded-particle model for rock. Int J Rock Mech Min Sci 41(8):1329–1364

Ritchie AM (1963) Evaluation of rock fall and its control. Highway Res. Rec. 17, HRB, National Research Council, Washington, pp 13–28

Spadari M, Giacomini A, Buzzi O, Fityus S, Giani GP (2012) In situ rockfall testing in New South Wales, Australia. Int J Rock Mech Min 49:84–93

Stahl M, Konietzky H (2011) Discrete element simulation of ballast and gravel under special consideration of grain-shape, grain-size and relative density. Granul Matter 13(4):417–428

Taghavi R (2011) Automatic clump generation based on mid-surface. Int. Conf. on Continuum and Distinct Element Numerical Modeling in Geomechanics, vol 1. Melbourne

Tagliavini F, Reichenbach P, Maragna D, Guzzetti F, Pasuto A (2009) Comparison of 2-D and 3-D computer models for the M. Salta rock fall, Vajont Valley, northern Italy. GeoInformatica 13:323–337

Thoeni K, Giacomini A, Lambert C, Sloan SW, Carter JP (2014) A 3D discrete element modelling approach for rockfall analysis with drapery systems. Int J Rock Mech Min Sci 68:107–119

Wadell H (1932) Volume shape and roughness of rock particles. J Geol 40:443–451

Wang B, Cavers DS (2008) A simplified approach for rockfall ground penetration and impact stress calculations. Landslides 5(3):305–310

Wang IT, Lee CY (2010) Influence of slope shape and surface roughness on the moving paths of a single rockfall. World Acad Sci Eng Technol 65:1021–1027

Wei LW, Chen H, Lee CF, Huang WK., Lin ML, Chi CC, Lin, HH (2014) The mechanism of rockfall disaster: A case study from Badouzih, Keelung, in northern Taiwan. Eng Geol 183:116–126

Wensrich CM, Katterfeld A (2012) Rolling friction as a technique for modelling particle shape in DEM. Powder Technol 217:409–417

Wyllie DC (2014) Rock fall engineering: development and calibration of an improved model for analysis of rock fall hazards on highways and railways. Ph.D. thesis, University of British Columbia, Vancouver

Zhang M, Yin Y (2013) Dynamics, mobility-controlling factors and transport mechanisms of rapid long-runout rock avalanches in China. Eng Geol 167(1):37–58

G. Gao · M. A. Meguid (✉)
Civil Engineering and Applied Mechanics,
McGill University,
817 Sherbrooke St. W., Montreal, QC H3A 0C3, Canada
e-mail: mohamed.meguid@mcgill.ca

G. Gao
e-mail: ge.gao2@mail.mcgill.ca